International Journal of Biological Macromolecules 133 (2019) 964–970

Contents lists available at ScienceDirect

International Journal of Biological Macromolecules

journal homepage: http://www.elsevier.com/locate/ijbiomac

Synthesis and characterization of porous tree gum grafted copolymer derived from *Prunus cerasifera* gum polysaccharide

Zhengjun Shi [a,b], Chengxinzhuo Jia [c], Dawei Wang [a,b,*], Jia Deng [a,b], Gaofeng Xu [a,b], Chunhua Wu [a,b], Mengyao Dong [d,e], Zhanhu Guo [d,**]

[a] Key Laboratory for Forest Resources Conservation and Utilization in the Southwest Mountains of China, Ministry of Education, Southwest Forestry University, Kunming 650224, China
[b] School of Chemical Engineering, Southwest Forestry University, Kunming 650224, China
[c] Eco-development Academy, Southwest Forestry University, Kunming, Yunnan 650224, China
[d] Integrated Composites Laboratory (ICL), Department of Chemical & Biomolecular Engineering, University of Tennessee, Knoxville, TN 37996, USA
[e] Key Laboratory of Materials Processing and Mold (Zhengzhou University), Ministry of Education, National Engineering Research Center for Advanced Polymer Processing Technology, Zhengzhou University, Zhengzhou, China

ARTICLE INFO

Article history:
Received 5 January 2019
Received in revised form 13 April 2019
Accepted 16 April 2019
Available online 17 April 2019

Keywords:
Polysaccharide
Prunus cerasifera
Grafted copolymerization
Thermal stability
Swelling capacity

ABSTRACT

Porous grafted copolymer with excellent thermal stability and swelling capacity was synthesized from water soluble *Prunus cerasifera* gum polysaccharide (PG) and acrylamide (AM). The monosaccharide compositions and the structure of *Prunus cerasifera* tree gum were detected by a high-performance anion exchange chromatography (HPAEC) system and ^{1}H NMR and ^{13}C NMR, and the obtained PG-AM copolymer was characterized by Fourier transform infrared (FT-IR), scanning electron microscope (SEM), thermogravimetric analysis (TGA) and differential scanning calorimetry (DSC), respectively. The results indicated that the water soluble polysaccharides obtained from *Prunus cerasifera* tree gum were mainly composed of L-arabinose (39.78%) and D-galactose (40.59%) with minor amount of xylose, mannose and uronic acids. The maximum percent and the grafting efficiency of grafting acrylamide (AM) onto PG to form PG-AM were obtained by copolymerization between polysaccharide and 3 times (weight) acrylamide with 3 mmol/L potassium persulfate initiator at 50 °C for 1 h. In addition, lots of isolated and conjoint pores were observed in the prepared PG-AM materials, with a diameters distribution between 2 and 10 μm. Compared with PG, the synthesized copolymer PG-AM showed an excellent performance in thermal stability and swelling capacity. The detailed structural characteristic together with excellent thermal stability and swelling properties will benefit efficient utilization of the synthesized copolymer as a precursor for preparation of large-scale environmentally friendly advanced materials with various potential applications.

1. Introduction

Tree gum exudates are usually produced by the trunk, branches, and fruits, as a self-protection method in response to the injury or microbial invasion [1–4]. Previous studies on the chemical structure of many plant gums showed that the tree gum exudates are mainly composed of hetero polysaccharides with complex structures and various monosaccharides [5–8]. The wide industrial applications of tree gum are due to its water-retention capacity to produce gels and its ability to enhance the stability of emulsions. For example, the gum arabic has been used in food industry as natural stabilizer or emulsifiers [9]. Besides, cashew gum has various applications in the agro-food, paper, cosmetic and pharmaceutical industries [10].

Recently, tree gum has been reported to be used as encapsulant and emulsifier in food industry, and as potential alternative to replace gum arabic in many fields of applications [11]. The species of genus *Prunus* produce copious gum exudates, among which peach (such as *P. persica*) gum is the most studied [7,12]. The studies on peach gum revealed that its main monosaccharide compositions were arabinose and galactose, and it also contained small amount of mannose, xylose, rhamnose and uronic acid [7,13]. *Prunus cerasifera* tree (*Prunus cerasifera Ehrhar F. atropurpurea*) is a common species of virescence tree in China. The *Prunus cerasifera* tree gum (PG) is a mucosity liquid with high clarity or with a light yellow color.

Polysaccharide based materials, especially natural polysaccharide as a potential substitute for non-degradable materials, have received increasing attention owing to their biodegradable, easily available, low cost, nontoxic and biocompatible characteristics [14]. Presently, the

* Correspondence to: D. Wang, School of Chemical Engineering, Southwest Forestry University, Kunming 650224, China.
** Corresponding author.
E-mail addresses: wdwchem@163.com (D. Wang), zguo10@utk.edu (Z. Guo).

https://doi.org/10.1016/j.ijbiomac.2019.04.128
0141-8130/

Table 1
Monosaccharide compositions and contents in the isolated PG polysaccharide fractions.

Samples	Monosaccharide	Abbreviation	Retention time (min)	Concentration (mg/L)	Relative content (%)
1	L-arabinose	Ara	10.28	23.62	39.78
2	D-galactose	Gal	13.02	24.11	40.59
3	D-glucose	Glu	15.10	0.19	0.32
4	D-xylose	Xyl	17.80	4.36	7.34
5	D-mannose	Man	18.77	1.87	3.15
6	D-glucuronic acid	GluA	31.68	1.31	2.21
7	D-galacturonic acid	GalA	34.45	3.93	6.62

natural polysaccharides including starch [15,16], dextrin [17], chitosan [18], cellulose [19], guar gum [20], and cashew gum [21] have been used to synthesize high absorbent resins via graft copolymerization reactions. Because the natural polysaccharides have favorable water absorb properties in themselves, they will soon form sol after dissolved in water. Therefore, they can easily react with many monomers, such as acrylamide, to yield the graft copolymerization products. As far as we know, the studies about *Prunus cerasifera* tree gum and its modified derivatives have not been reported in literature.

In this article, the monosaccharide compositions of PG polysaccharide were analyzed by a high-performance anion exchange chromatography (HPAEC) system, and the structure of the PG polysaccharide was characterized by ^{1}H NMR and ^{13}C NMR spectral analyses. The grafted copolymer was prepared by reacting PG with acrylamide monomer in the existence of potassium persulfate (PPS) initiator. The grafted copolymer was characterized by FT-IR spectroscopy, scanning electron microscope, thermogravimetric analysis and differential scanning calorimetry. Besides, the water absorption capacity of synthesized grafted copolymer was also tested. The structure of *Prunus cerasifera* tree gum was studied for the first time, and the graft copolymerization of this polysaccharide was also carried out.

2. Materials and methods

2.1. Materials

Prunus cerasifera tree gum (PG) was collected from the trunk of *Prunus cerasifera* trees in the campus of Southwest Forestry University, Kunming, China, and air-dried (Fig. S1). The raw gum was further purified with distilled water to obtain water-soluble polysaccharide using the previously reported method with some modifications [13,22]. In detail, 20 g raw gum was extracted with 1 L distilled water at 60 °C under agitation for 2 h. The supernatant was collected by centrifugation, concentrated using a vacuum rotary evaporator, and then poured into ethanol. The precipitates were collected as water soluble polysaccharides by centrifugation and freeze-drying. The chemical reagents acrylamide (AM), potassium persulfate, sulfuric acid, acetone and ethyl alcohol used in experiments were analytical R grade, and all the chemicals were purchased from Sinopharm Chemical Reagent Co., Ltd., Shanghai China.

2.2. Graft copolymerization of PG with acrylamide

The grafted copolymer was prepared by free radical grafting polymerization between water soluble polysaccharides and acrylamide. Briefly, 0.5 g polysaccharide and 0.5 to 4.0 g acrylamide were dispersed in 50 mL distilled water in a 250 mL round-bottomed flask in nitrogen gas atmosphere and stirred for 60 min. Then, 1 to 5 mmol/L potassium persulfate (PPS) solution was added to the solution as initiator to evaluate the effect of PPS concentration on the polymerization. Polymerizations were conducted at 20, 30, 40, 50, 60 and 80 °C for 3 h, respectively. At the end of reaction, the solutions were cooled down to room temperature and precipitated in acetone. The precipitates were collected by filtration, washed with 3 mL ethanol for three times, refluxed with acetone for 20 h to remove the homopolymer and unreacted monomers, and then dried in vacuum at 40 °C. The percent of grafting (Pg) and grafting efficiency (GE) were calculated according to literature as follows [17,23]:

$$\mathrm{Pg} = \frac{Weight\ of\ PG{-}AM{-}Weight\ of\ PG}{Weight\ of\ PG} \times 100 \quad (1)$$

$$\mathrm{GE} = \frac{Weight\ of\ PG{-}AM{-}Weight\ of\ PG}{Weight\ \ of monomer\ charged} \times 100 \quad (2)$$

2.3. Analysis methods

2.3.1. Chemical composition

The structural study is a basic requirement for understanding the physical behaviors of gums. The structural features of PG polysaccharide were revealed by monosaccharide composition analysis and NMR spectra. The monosaccharide compositions of the PG polysaccharide fraction were determined by hydrolysis with dilute sulfuric acid according to the

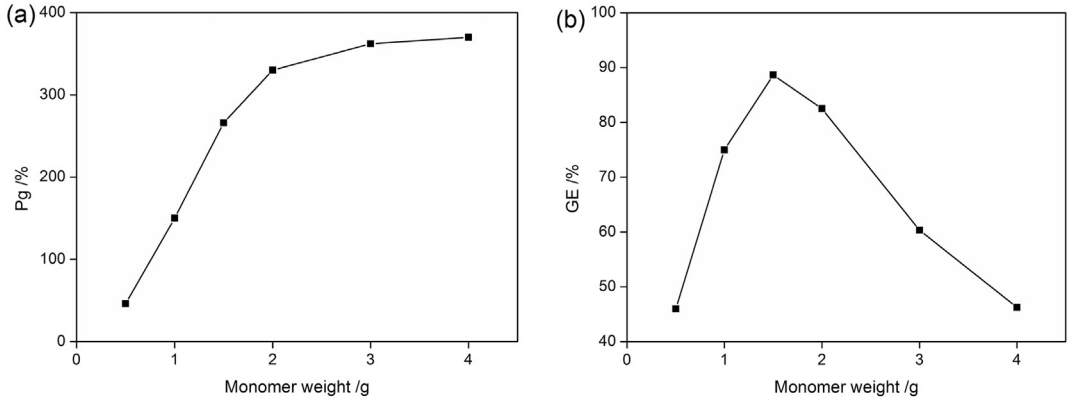

Fig. 1. Effect of monomer amount on the Pg (a) and GE (b) of grafted copolymer: Weight of PG = 0.5 g, concentration of initiator (PPS) = 2 mmol/L, t = 180 min, T = 50 °C.

published procedures [24]. Briefly, 5 mg polysaccharides were hydrolyzed with 1.480 mL 1 mol/L H_2SO_4 for 2.5 h at 105 °C. At the end of acid hydrolysis, the mixture was filtered, diluted and analyzed by high-performance anion exchange chromatography (HPAEC) system (Dionex ICS 3000, U.S.), which was equipped with a pulsed amperometric detector and an ion exchange Carbopac PA-1 columm (4 × 250 mm). The chemical compositions were separated in 18 mmol/L NaOH (carbonate free and purged with nitrogen) with post-column addition of 0.30 mol/L NaOH at 0.5 mL/min in 45 min, followed by 10 min elution with 0.2 mol/L NaOH. Then, the elution with 18 mmol/L NaOH for 15 min was used to re-equilibrate the column. Calibration was performed with standards of L-rhamnose, L-arabinose, D-glucose, D-galactose, D-mannose, D-xylose, glucuronic acid and galacturonic acid. All the analyses experiments were run twice, and the average values were calculated for all the polysaccharide fractions.

2.3.2. ^1H NMR and ^{13}C NMR spectra for PG polysaccharide

^1H NMR and ^{13}C NMR spectra were obtained using a 600 MHz Bruker Avance spectrometer. The sample (25 mg) was dissolved in D_2O (3 mL) at 60 °C before detection. The chemical shifts of the sample were calibrated using tetramethylsilane (TMS) as an internal standard.

2.3.3. Characterization of graft copolymerization product

Fourier transform infrared (FT-IR) spectra of the PG polysaccharide and graft copolymerization product PG-AM were obtained on a Varian 640-IR FT-IR spectrometer, and a KBr pellets method was used in the test. Before data collection, a background scanning was performed for background correction, and the spectra were recorded in the range of 500–4000 cm^{-1}. A Hitachi S-3000 N scanning electron microscope (SEM) was used to characterize the morphology of the PG-AM grafted copolymer at an accelerating voltage of 15.0 kV. The thermal properties of samples were measured with a Mettler Toledo TGA/DSC instrument from room temperature to 700 °C at a heating rate of 10 °C min^{-1} under a dynamic nitrogen atmosphere.

2.3.4. Swelling study

Water absorption capacity test was conducted according to the reported method [18]. Briefly, 0.2 g sample of PG or PG-AM was soaked in 50 mL distilled water for 30, 60, 90, 120, 150, 180, 210 and 240 min, respectively. At the end of the time, the samples were filtered using a 100-mesh screen and drained on the sieve for 15 min to remove the redundant water, and then weighted. Percent swelling (Ps) was calculated by the following expression [17,23,25]:

$$P_S = \frac{Weight\ of\ swollen\ polymer - Weight\ of\ dry\ polymer}{Weight\ of\ dry\ polymer} \times 100 \qquad (3)$$

3. Results and discussion

3.1. Structural characterization of PG polysaccharide

3.1.1. Monosaccharide and uronic acid composition analyses

The chemical composition of water soluble polysaccharides from PG is shown in Table 1. Both Gal and Ara are observed obviously to be the main neutral sugars followed by Xyl, uronic acids and Man, and minimum amount of Glu. This result suggested that arabinogalactan was the main backbone of the water soluble polysaccharides substituted with Xyl and uronic acids side chains. It was in agreement with the previously reported structure of polysaccharides from peach gum (*Prunus persica*) [3,7].

3.1.2. NMR spectral analysis

The detailed structural features of polysaccharides were further illustrated by ^1H NMR and ^{13}C NMR. The ^1H and ^{13}C NMR spectra show the signals of different intensities, indicating that the polysaccharides

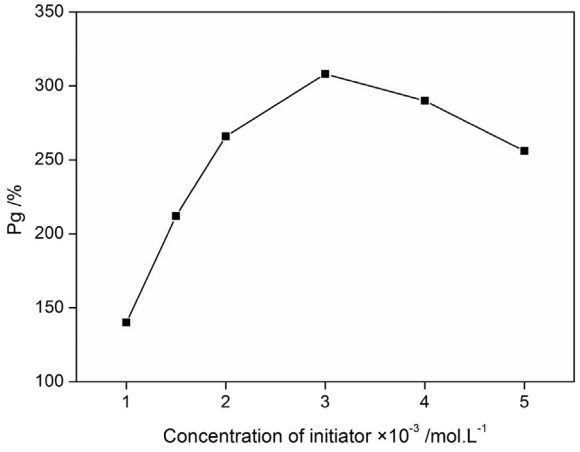

Fig. 2. Effect of initiator concentration on the Pg of grafted copolymer: Weight of PG = 0.5 g, weight of AM = 1.5 g, t = 180 min, T = 50 °C.

are structurally heterogeneous [26]. The ^1H chemical shifts of the structural features of polysaccharides are shown in Fig. S2. The signals in the range of 3.3–5.5 ppm were assigned to the proton in polysaccharides [27]. The strong peaks in the range of 3.3–4.5 ppm indicated that β-pyranose was the main component in the polysaccharide [28].

Generally, in the ^{13}C NMR spectrum of carbohydrate, the anomeric carbon (C-1) signals of glycosides are assigned to δ 90–115 ppm, while the signals of C-2, C-3, C-4, C-5, and C-6 from the glycosidic ring are assigned to δ 60–90 ppm [27,29]. As shown in Fig. S3, the dominant peak at δ 104.4 ppm is from β-D-Gal*p* units, and the very strong peak at 60.3 ppm is assigned to C-6 of Gal*p* units [3,24]. This reveals the presence of a major β-(1,6)-linked D-Gal*p* backbone. The signals at δ 112.4–111.2 ppm are ascribed to C-1 of α-L-Ara*f* units, while the two peaks at δ 79.2 and 71.4 can be assigned to C-3 and C-5 of α-L-Ara*f* units [3]. The above NMR analyses revealed that the polysaccharide extracted from PG may have an arabinogalactan main chain, which is in agreement with the monosaccharide and uronic acids analysis. However, the exact structure of PG polysaccharides has not been established because of its complexity. Previous studies have shown that, the polysaccharide components of several fruit-bearing tree gums from genus *Prunus* belong to the arabinogalactan group [30]. Recent studies revealed that, the core structures of the polysaccharide of peach gum were possibly a highly branched polysaccharide with mixed (1,3)- and (1,6)-linked Gal*p* units [7]. Similarly, the PG polysaccharides also has a (1,6)-linked D-Gal*p* backbone which forms an arabinogalactan main chain.

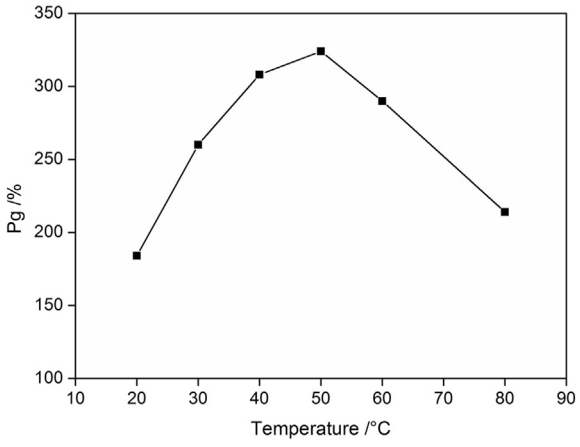

Fig. 3. Effect of temperature on the Pg of grafted copolymer: Weight of PG = 0.5 g, weight of AM = 1.5 g, concentration of initiator (PPS) = 3 mmol/L, t = 180 min.

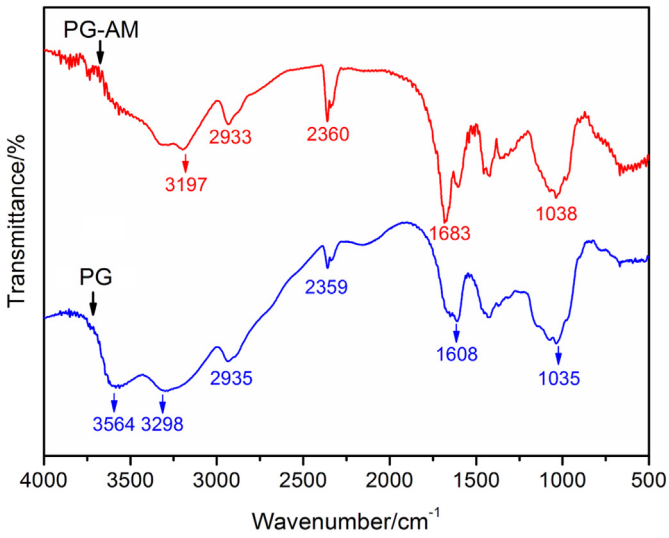

Fig. 4. FT-IR spectra of PG polysaccharide and PG-AM grafted copolymer.

3.2. Effect of reaction parameters on grafting of AM onto PG

3.2.1. Effect of monomer dosage

The effect of AM monomer to PG ratio on the grafting percent was conducted in the range of 1 to 8, keeping other variables fixed (PG = 0.5 g, concentration of initiator (PPS) = 2 mmol/L, t = 180 min, T = 50 °C). As this ratio increases from 1 to 4, the Pg of PG obviously increases from 46% to 330%. Further increasing the dosage of AM to 8 times of PG, a slight increment of Pg to 370% is obtained (Fig. 1a). However, the GE increases from 46.0% to 88.7% and then decreases to 46.3%, with the maximum of GE at AM to PG ratio of 3 (Fig. 1b), under the same reaction conditions. The early increasing trend of Pg and GE may be due to the availability of additional monomers for copolymerization. However, at a higher monomer dosage, the decrease of GE could be attributed to the consumption of monomers to form more homopolymer [18]. A similar observation was reported previously [23].

3.2.2. Effect of initiator concentration

Fig. 2 illustrates the effect of potassium persulfate (PPS) initiator concentration on the Pg. The Pg increases from 140% to 308% and decreases to 256% as the concentration of PPS increases from 1 to 3 mmol/L and further increases to 5 mmol/L. These results may be ascribed to the fact that high PPS concentration provides more primary free radicals to react with PG molecules [23]. However, further aggregating of primary free radicals could accelerate the reaction of PPS and radicals, terminating the chain propagation reaction and decreasing the Pg value [18].

3.2.3. Effect of reaction temperature

The grafting reactions were carried out between 20 and 80 °C to evaluate the effect of temperature on the Pg. As shown in Fig. 3, the P_g value increases significantly as the reaction temperature increases from 20 to 50 °C. The optimum P_g (324%) and GE (108%) were observed at 50 °C. However, a further increase in temperature decreases the P_g. There exists an optimum temperature to afford a maximum graft yield, below this temperature, the decomposition of initiator and the diffusion processes are not adequate to yield high graft levels [31]. Increasing temperature could promote the copolymerization, but homopolyerization of AM occurred at high reaction temperature.

3.3. FT-IR spectra and SEM morphologies

Fig. 4 shows the FT-IR spectra of PG and PG-AM. For the PG sample, the absorption peaks at around 3250–3750 cm^{-1} can be ascribed to the stretching vibration of hydroxyl group (–OH), while the peak at 1608 cm^{-1} is assigned to the bending vibration of hydroxyl group [32]. In the FT-IR spectrum of grafted copolymer PG-AM, the strong peak at 1683 cm^{-1} is ascribed to the stretching vibration of carbonyl group (C=O) [33]. The presence of C=O group in PG-AM indicated the formation of grafted copolymer.

Fig. 5 shows the SEM morphologies of PG-AM grafted copolymer. Lots of isolated and conjoint pores are observed on the surface of PG-AM materials. The diameters of most honeycomb-like pores are distributed between 2 and 10 μm. The porous structure of PG-AM is closely associated with its swollen capacity.

3.4. Thermal properties of PG and PG-AM

The thermal properties of PG and PG-AM were examined by thermogravimetric analysis (TGA) and differential scanning calorimetry (DSC). As shown in Fig. 6a, the slight weight loss of PG and PG-AM samples below 200 °C corresponds to the evaporation of absorbed water. The decomposition of the polysaccharide PG was observed in the region at about 200–400 °C with a weight loss of 58.5%, which was probably assigned to the degradation of the branches [22]. As compared to the PG, the PG-AM degraded at a relatively higher temperature. Two steps of weight loss were observed at about 300 and 400 °C, which might be ascribed to the degradation of sugar and AM branches, respectively. As the temperature increased to 700 °C, there were still 9.56% and 13.67% solid residues left for PG and PG-AM, respectively. These results suggest a higher thermal stability of PG-AM than that of PG.

Fig. 6b shows the DSC curves of PG and PG-AM. The PG sample showed two intense exothermic process with the peak temperature of

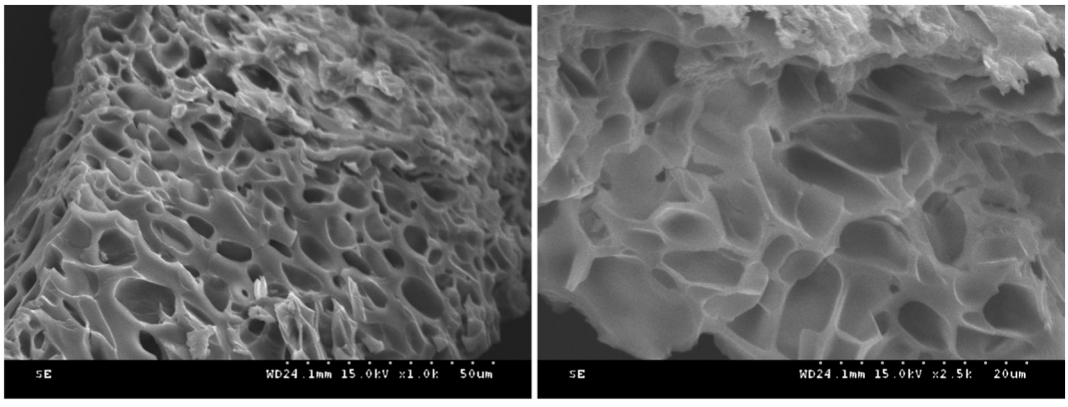

Fig. 5. SEM images of grafted copolymer PG-AM.

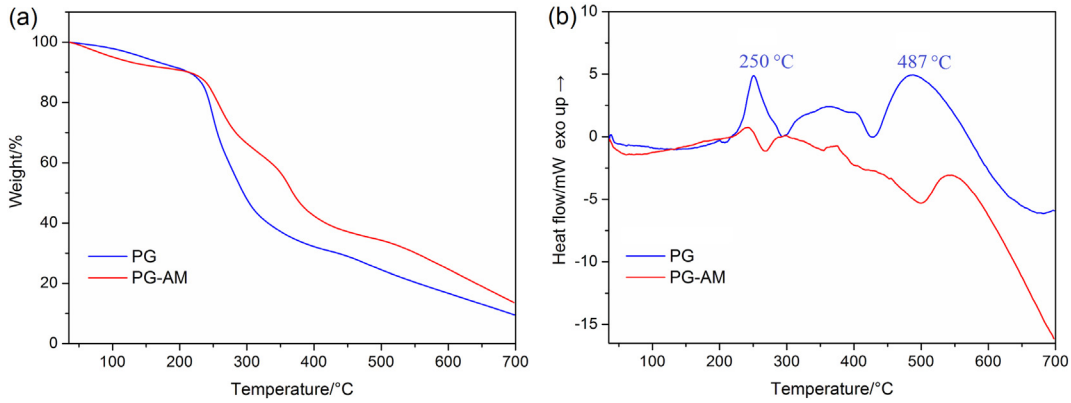

Fig. 6. TGA curves (a) and DSC curves (b) for PG and PG-AM.

250 and 487 °C, respectively. The two exothermic process of PG sample may be attributed to the decomposition of branches (250 °C) and main chain (487 °C) of the polysaccharide. However, the PG-AM has no obvious exothermic peak during the whole decomposition process (Fig. 6b). Based on the above results, a higher thermal stability and a lower exothermic property indicated a more stable molecular structure of PG-AM copolymer, which is mainly from the grafting of AM onto polysaccharide molecules of PG.

3.5. Swelling capacity of PG-AM copolymers

Fig. 7 depicts the swelling curves of PG and PG-AM. The samples (PG, PG-AM-1 and PG-AM-2) were swelled and adsorbed most of water within 120 min, obtaining a Ps as 684, 608 and 448, respectively. This result indicated that copolymers had a better swelling capacity than PG. However, the increase rate of Ps is gradually slowing down after swelling for 120 min. A more favorable swelling capacity of PG-AM-1 than PG-AM-2 may result from the Pg and GE values of samples. It suggested that the swelling capacity of the copolymer was positively correlated with the number of polyacrylamide side chains. In addition, the porous structure of grafted copolymer PG-AM may also play an important role in water absorption process, and greatly enhance the swelling capacity.

Graft copolymerization is an appropriate technique for modifying the chemical and physical properties of natural polysaccharides. In addition to improving the swelling capacity of polysaccharide, it is possible to develop efficient, shear stable, thermally stable and biodegradable polymers for industrial applications by grafting of flexible polyacrylamide (PAM) chains onto the polysaccharide backbone [34]. In the present research, the synthesized PG-AM copolymer is expected to be developed into an environmentally friendly resin with a high absorbent quality according to excellent thermal stability and swelling capacity. Besides, the prepared porous polymers with good thermal stability can also be used as host matrix for the preparation of functional composites and gels [35–61].

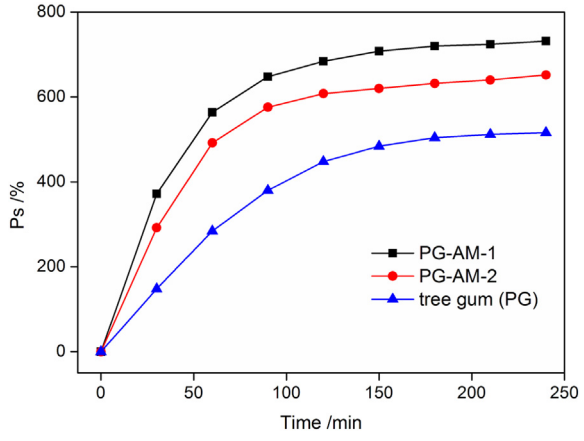

Fig. 7. Swelling capacity of tree gum (PG) and grafted copolymer (PG-AM) at room temperature: For PG-AM-1, Pg = 266, GE = 88.7; For PG-AM-2, Pg = 150, GE = 75.

4. Conclusions

Water soluble polysaccharides from tree gum are composed of arabinogalactan backbone and xylose, mannose and uronic acids side chains. The modification of these polysaccharides with acrylamide yielded a copolymer with a great performance in thermal stability and swelling capacity. The optimum copolymerization conditions were found to be acrylamide to polysaccharides at a ratio of 3:1 with 3 mmol/L PPS initiator at 50 °C. After copolymerization, the swelling capacity of PG increased with increasing the grafting percent and yielded a maximum enhancement as 52.7%. This study lays a foundation for the applications of *Prunus cerasifera* tree gum The copolymer synthesized from natural polysaccharides, which shows excellent performance in thermal stability and swelling capacity, can therefore be used as a precursor for preparation of a possibly large-scale advanced materials, and can be combined with other functional materials like metals [62–72], ceramics [73–78] and nanocarbons [79–85] for various applications including drug delivery, nutrition carrier, absorbent resin, polymer nanocomposties.

Acknowledgements

The work was financially supported by National Natural Science Foundation of China (31460214, 31560195, 31760195), Fundamental Research Funds of Yunnan Province, China (2018FB066), and Guanxi Key Laboratory of Chemistry and Engineering of Forest Products, China (2017AD19029).

Appendix A. Supplementary data

Supplementary data to this article can be found online at https://doi.org/10.1016/j.ijbiomac.2019.04.128.

References

[1] M.R. Marques, J. Xavier-Filho, Enzymatic and inhibitory activities of cashew tree gum exudate, Phytochemistry 30 (1991) 1431–1433.
[2] T.G. Beckman, P.L. Pusey, P.F. Bertrand, Impact of fungal gummosis on peach trees, Hortscience 38 (2003) 1141–1143.
[3] F.F. Simas-Tosin, R.R. Barraza, C.L.O. Petkowicz, J.L.M. Silveira, G.L. Sassaki, E.M.R. Santos, P.A.J. Gorin, M. Iacomini, Rheological and structural characteristics of peach tree gum exudate, Food Hydrocolloid 24 (2010) 486–493.
[4] V. Rana, P. Rai, A.K. Tiwary, R.S. Singh, J.F. Kennedy, C.J. Knill, Modified gums: approaches and applications in drug delivery, Carbohyd. Polym. 83 (2011) 1031–1047.
[5] H. Mirhosseini, B.T. Amid, A review study on chemical composition and molecular structure of newly plant gum exudates and seed gums, Food Res. Int. 46 (2012) 387–398.

[6] T.M. Silva, P.O. Santiago, L.L.A. Purcena, K.F. Fernandes, Study of the cashew gum polysaccharide for the horseradish peroxidase immobilization structural characteristics, stability and recovery, Mat. Sci. Eng. C-Mater. 30 (2010) 526–530.

[7] F.F. Simas, P.A.J. Gorin, R. Wagner, G.L. Sassaki, A. Bonkerner, M. Iacomini, Comparison of structure of gum exudate polysaccharides from the trunk and fruit of the peach tree (Prunus persica), Carbohyd. Polym. 71 (2008) 218–228.

[8] P. Somboonpanyakul, Q. Wang, W. Cui, S. Barbut, P. Jantawat, Malva nut gum. (Part I): extraction and physicochemical characterization, Carbohyd. Polym. 64 (2006) 247–253.

[9] N.A. Almuslet, E.A. Hassan, A.S. Al-Sherbini, M. Muhgoub, Diode laser (532 nm) induced grafting of polyacrylamide onto gum arabic, J. Phys. Sci. 23 (2012) 43–53.

[10] T.M. Silva, P.O. Santiago, L.L. Purcena, K.F. Fernandes, Study of the cashew gum polysaccharide for the horseradish peroxidase immobilization-structural characteristics, stability and recovery, Mat. Sci. Eng. C - Mater. 30 (2010) 526–530.

[11] B.C. Porto, M. Cristianini, Evaluation of cashew tree gum (Anacardium occidentale L.) emulsifying properties, LWT - Food Sci. Technol. 59 (2014) 1325–1331.

[12] J.C. Huang, L. Zhou, Peach gum polysaccharide polyelectrolyte: preparation, properties and application in layer-by-layer self-assembly, Carbohyd. Polym. 113 (2014) 373–379.

[13] H.F. Qian, S.W. Cui, Q. Wang, C. Wang, H.M. Zhou, Fractionation and physicochemical characterization of peach gum polysaccharides, Food Hydrocolloid 25 (2011) 1285–1290.

[14] R.C. Mundargi, S.A. Patil, T.M. Aminabhavi, Evaluation of acrylamide-grafted-xanthan gum copolymer matrix tablets for oral controlled delivery of antihypertensive drugs, Carbohyd. Polym. 69 (2007) 130–141.

[15] X.F. Ma, X.Y. Liu, D.P. Anderson, P.R. Chang, Modification of porous starch for the adsorption of heavy metal ions from aqueous solution, Food Chem. 181 (2015) 133–139.

[16] H. El-Hamshary, F.N. Assubaie, Synthesis of cationic and ampholytic starch graft acrylamide and their aqueous salt absorption, J. Macromol. Sci. A 48 (2011) 454–461.

[17] R.K. Sharma, Lalita, G.S. Chauhan, R. Verma, Graft copolymers of acrylonitrile onto dextrin for use in separation technologies, Int. J. Polym. Mater. 59 (2010) 263–285.

[18] A.J.M. Al-Karawi, Z.H.J. Al-Qaisi, H.I. Abdullah, A.M.A. Al-Mokaram, D.T.A. Al-Heetimi, Synthesis, characterization of acrylamide grafted chitosan and its use in removal of copper(II) ions from water, Carbohyd. Polym. 83 (2011) 495–500.

[19] N.H. Zhai, W.B. Wang, A.Q. Wang, Synthesis and swelling characteristics of a pH responsive guar gum-g-poly(sodium acrylate)/medicinal stone superabsorbent composite, Polym. Compos. 32 (2011) 210–218.

[20] V.S. Pandey, S.K. Verma, K. Behari, Graft [partially carboxymethylated guar gum-g-poly N-(hydroxymethyl) acrylamide] copolymer: from synthesis to applications, Carbohyd. Polym. 110 (2014) 285–291.

[21] D.A. Silva, R.C. Paula, J.P. Feitosa, Graft copolymerisation of acrylamide onto cashew gum, Eur. Polym. J. 43 (2007) 2620–2629.

[22] H.Y. Yang, D.W. Wang, J. Deng, J. Yang, C. Shi, F.L. Zhou, Z.J. Shi, Activity and structural characteristics of peach gum exudates, Int. J. Polym. Sci. (2018) doi.org/https://doi.org/10.1155/2018/4593735.

[23] T.K. Giri, M. Pradhan, D.K. Tripathi, Synthesis of graft copolymer of kappa-carrageenan using microwave energy and studies of swelling capacity, flocculation properties, and preliminary acute toxicity, Turk. J. Chem. 40 (2016) 283–295.

[24] J. Deng, Z.J. Shi, X.Z. Li, H.M. Liu, Soluble polysaccharide isolation and characterization from rabbiteye blueberry (*Vaccinium ashei*) fruits, BioResources 8 (2013) 405–419.

[25] K. Sharma, B.S. Kaith, V. Kumar, S. Kalia, V. Kumar, H.C. Swart, Water retention and dye adsorption behavior of Gg-cl-poly(acrylic acid-aniline) based conductive hydrogels, Geoderma 232 (2014) 45–55.

[26] E.L. Zdorovenko, A.S. Shashkov, A.A. Kadykova, E.P. Kiseleva, V.V. Savich, G.I. Novik, Y.A. Knirel, Structural analysis of the O-polysaccharide from the lipopolysaccharide of *Pseudomonas putida* BIM B-1100, Carbohydr. Res. 465 (2018) 58–65.

[27] H.Y. Yang, X.L. Song, T.Q. Yuan, F. Xu, R.C. Sun, Fractional characterization of hemicellulosic polymers isolated from *Caragana korshinskii* Kom, Ind. Eng. Chem. Res. 50 (2011) 6877–6885.

[28] Y.C. Lin, X.Y. Wu, S. Feng, G.C. Jiang, S.N. Zhou, L.L.P. Vrijmoed, E.B.G. Jones, A novel *N*-cinnamoylcyclopeptide containing an allenic ether from the fungus Xylaria sp. (strain #2508) from the South China Sea, Tetrahedron Lett. 42 (2001) 449–451.

[29] M.L.C. Gonzaga, N. Ricardo, F. Heatley, S.A. Soares, Isolation and characterization of polysaccharides from *Agaricus blazei* Murill, Carbohyd. Polym. 60 (2005) 43–49.

[30] A.M. Stephen. Other plant polysaccharides. In G.O. Aspinall (Ed.) The Polysaccharides (Vol. vol. 2, pp. 97–180). New York, NY: Academic press.

[31] R.K. Sharma, Lalita, G.S. Chauhan, R. Verma, Graft copolymers of acrylonitrile onto dextrin for use in separation technologies, Int. J. Polym. Mater. 59 (2010) 263–285.

[32] J.L. Wang, W.B. Wang, A.Q. Wang, Synthesis characterization and swelling behaviors of hydroxyethyl cellulose-g-poly(acrylic acid)/attapulgite superabsorbent composite, Polym. Eng. Sci. 50 (2010) 1019–1027.

[33] M.M. Fares, A.S. El-faqeeh, M.E. Osman, Graft copolymerization onto starch-I. synthesis and optimization of starch grafted with N-tert-Butylacrylamide copolymer and its hydrogels, J. Polym. Res. 10 (2003) 119–125.

[34] B.R. Nayak, R.P. Singh, Synthesis and characterization of grafted hydroxypropyl guar gum by ceric ion induced initiation, Eur. Polym. J. 37 (2001) 1655–1666.

[35] Q. Chen, L. Zhu, C. Zhao, Q.M. Wang, J. Zheng, A robust, one-pot synthesis of highly mechanical and recoverable double network hydrogels using thermoreversible sol-gel polysaccharide, Adv. Mater. 25 (2013) 4171–4176.

[36] Y.X. Zhang, B.P. Ren, F.Y. Yang, Y.Q. Cai, H. Chen, T. Wang, Z.Q. Feng, J.X. Xu, J. Zheng, Micellar-incorporated hydrogels with highly tough, mechanoresponsive, and self-recovery properties for strain-induced color sensors, J. Mater. Chem. C 6 (2018) 11536–11551.

[37] H. Chen, Y.L. Liu, B.P. Ren, Y.X. Zhang, J. Ma, L.J. Xu, Q. Chen, J. Zhang, Super bulk and interfacial toughness of physically crosslinked double-network hydrogels, Adv. Funct. Mater. 27 (2017), 1703086.

[38] X.Y. Wu, W. Li, P. Wu, C.H. Ma, Y.S. Liu, M.C. Xu, S.X. Liu, Long-lived room-temperature phosphorescent nitrogen-doped CQDs/PVA composites: fabrication, characterization and application, Eng. Sci. 4 (2018) 111–118.

[39] T. Liang, L. Qi, Z. Ma, Z. Xiao, Y. Wang, H. Liu, J. Zhang, Z. Guo, C. Liu, W. Xie, T. Ding, N. Lu, Experimental study on thermal expansion coefficient of composite multi-layered flaky gun propellants, Compos. Part B 166 (2019) 428–435.

[40] X. Li, S. Zhao, W. Hu, X. Zhang, L. Pei, Z. Wang, Robust superhydrophobic surface with excellent adhesive properties based on benzoxazine/epoxy/mesoporous SiO_2, Appl. Surface Sci. 481 (2019) 374–378.

[41] D. Jiang, Y. Wang, B. Li, et al., Flexible sandwich structural strain sensor based on silver nanowires decorated self-healing substrate, Macromol. Mater. Eng. (2019) https://doi.org/10.1002/mame.201900074 in press.

[42] X. Liu, Y. Pan, G. Zheng, et al., Overview of the experimental trends in water-assisted injection molding, Macromol. Mater. Eng. 303 (8) (2018), 1800035.

[43] F. Luo, X. Liu, C. Yan, et al., Molecular orientation dependent dynamic viscoelasticity in uni-axially drawn polycarbonate, Polym. Testing 69 (2018) 528–535.

[44] T. Bai, B. Dong, M. Xiao, H. Liu, et al., Polystyrene foam with high cell density and small cell size by compression-injection molding and core back foaming technique: evolution of cells in cavity, Macromol. Mater. Eng. 303 (2018), 1800110.

[45] L. Ma, N. Li, G. Wu, G. Song, X. Li, P. Han, G. Wang, Y. Huang, Interfacial enhancement of carbon fiber composites by growing TiO_2 nanowires onto amine-based functionalized carbon fiber surface in supercritical water, Appl. Surf. Sci. 433 (2018) 560–567.

[46] R. Ma, Y. Wang, H. Qi, et al., Nanocomposite sponges of sodium alginate/graphene oxide/polyvinyl alcohol as potential wound dressing: in vitro and in vivo evaluation, Compos. Part B 167 (2019) 396–405.

[47] C. Wang, Z. He, X. Xie, et al., Controllable cross-linking anion exchange membranes with excellent mechanical and thermal properties, Macromol. Mater. Eng. 3 (2018) 1700462.

[48] J. Chen, S. Zhao, W. Hu, et al., Vinyl ester resin nanocomposites reinforced with carbon nanotubes modified basalt fibers, Sci. Adv. Mater. (2019)https://doi.org/10.1166/sam.2019.3558 in press.

[49] S. Shi, L. Wang, Y. Pan, et al., Remarkably strengthened microinjection molded linear low-density polyethylene (LLDPE) via multi-walled carbon nanotubes derived nanohybrid shish-kebab structure, Compos. Part B 167 (2019) 362–369.

[50] H. Gu, X. Xu, M. Dong, et al., Carbon nanospheres induced high negative permittivity in nanosilver-polydopamine metacomposites, Carbon 147 (2019) 550–558.

[51] G. Zhu, X. Cui, Y. Zhang, et al., Poly (vinyl butyral)/graphene oxide/poly (methylhydrosiloxane) nanocomposite coating for improved aluminum alloy anti-corrosion, Polymer (2019)https://doi.org/10.1016/j.polymer.2019.03.056 in press.

[52] Q. Hu, N. Zhou, K. Gong, et al., Intracellular polymer substances induced conductive polyaniline for improved methane production from anaerobic wastewater treatment, ACS Sustain. Chem. Eng. 7 (2019) 5912–5920.

[53] Q. Chen, Q. Yin, A. Dong, et al., Metal complex hybrid composites based on fullerene-bearing porous polycarbazole for H_2, CO_2 and CH_4 uptake and heterogeneous hydrogenation catalysis, Polymer 169 (2019) 255–262.

[54] X. Gong, Y. Liu, Y. Wang, et al., Amino graphene oxide/dopamine modified aramid fibers: preparation, epoxy nanocomposites and property analysis, Polymer 168 (2019) 131–137.

[55] J. Xu, K. Li, H. Deng, et al., Preparation of MCA-SiO_2 and its flame retardant effects on glass fiber reinforced polypropylene, Fibers Polym 20 (2019) 120–128.

[56] M. Liu, B. Li, H. Zhou, C. Chen, Y. Liu, T. Liu, Extraordinary rate capability achieved by a 3D "skeleton/skin" carbon aerogel-polyaniline hybrid with vertically aligned pores, Chem. Commun. 53 (2017) 2810–2813.

[57] M. Dong, Q. Li, H. Liu, et al., Thermoplastic polyurethane-carbon black nanocomposite coating: fabrication and solid particle erosion resistance, Polymer 158 (2018) 381–390.

[58] Z. Wu, S. Gao, L. Chen, et al., Electrically insulated epoxy nanocomposites reinforced with synergistic core-shell SiO_2@MWCNTs and montmorillonite bifillers, Macromol. Chem. Phys. 218 (2017), 1700357.

[59] Z. Wu, H. Cui, L. Chen, et al., Interfacially reinforced unsaturated polyester carbon fiber composites with a vinyl ester-carbon nanotubes sizing agent, Compos. Sci. Technol. 164 (2018) 195–203.

[60] H. Zhang, S. Lyu, X. Zhou, H. Gu, C. Ma, C. Wang, T. Ding, Q. Shao, H. Liu, Z. Guo, Super light 3D hierarchical nanocellulose aerogel foam with superior oil adsorption, J. Colloid Interf. Sci. 536 (2019) 245–251.

[61] H. Gu, H. Zhang, C. Ma, et al., Trace electrosprayed nanopolystyrene facilitated dispersion of multiwalled carbon nanotubes: simultaneously strengthening and toughening epoxy, Carbon 142 (2019) 131–140.

[62] Z. Zhao, P. Bai, L. Li, J. Li, L. Wu, P. Huo, L. Tan, The reaction thermodynamics during plating Al on graphene process, Materials 12 (2) (2019) 330.

[63] Y. Zhao, S. Deng, H. Liu, J. Zhang, Z. Guo, H. Hou, First-principle investigation of pressure and temperature influence on structural, mechanical and thermodynamic properties of Ti_3AC_2 (A = Al and Si), Comput. Mater. Sci. 154 (2018) 365–370.

[64] Z. Zhao, R. Guan, J. Zhang, Z. Zhao, P. Bai, Effects of process parameters of semisolid stirring on microstructure of Mg-3Sn-1Mn-3SiC (wt%) strip processed by rheo-rolling, Acta Metall. Sin. (Engl. Lett.) 30 (2017) 66–72.

[65] Z. Zhao, P. Bai, R. Misra, et al., AlSi10Mg alloy nanocomposites reinforced with aluminum-coated graphene: selective laser melting, interfacial microstructure and property analysis, J. Alloys Compounds 792 (2019) 203–214.

[66] Z. Zhao, J. Li, P. Bai, H. Qu, M. Liang, H. Liao, L. Wu, P. Huo, H. Liu, J. Zhang, Microstructure and mechanical properties of TiC-reinforced 316L stainless steel composites fabricated using selective laser melting, Metals 9 (2) (2019) 267.

[67] Y. Zhao, B. Zhang, H. Hou, W. Chen, M. Wang, Phase-field simulation for the evolution of solid/liquid interface front in directional solidification process, J. Mater. Sci. Technol. 35 (2019) 1044–1052.
[68] Y. Zhao, L. Qi, Y. Jin, K. Wang, J. Tian, P. Han, The structural, elastic, electronic properties and Debye temperature of D022-Ni3V under pressure from first-principles, J. Alloys Compounds 647 (2015) 1104–1110.
[69] Z. Zhao, P. Bai1, R. Guan, V. Murugadoss, H. Liu, X. Wang, and Z. Guo, Microstructural evolution and mechanical strengthening mechanism of Mg-3Sn-1Mn-1La alloy after heat treatments, Mater. Sci. Eng. A, 734 (2018) 200–209.
[70] Y. Zhao, X. Tian, B. Zhao, et al., Precipitation sequence of middle Al concentration alloy using the inversion algorithm and microscopic phase field model, Sci. Adv. Mater. 10 (2018) 1793–1804.
[71] Y. Zhao, F. Liu, J. Tan, et al., Preparation and hydrogen storage of Pd/MIL-101 nanocomposites, J. Alloys Compounds 772 (2019) 186–192.
[72] F. Liu, Z. Xu, Z. Wang, et al., Structures and mechanical properties of Nb-Mo-Co(Ru) solid solutions for hydrogen permeation, J. Alloys Compds 756 (2018) 26–32.
[73] R. Ge, S. Wang, J. Su, Y. Dong, Y. Lin, Q. Zhang, L. Chen, Phase-selective synthesis of self-supported RuP films for efficient hydrogen evolution electrocatalysis in alkaline media, Nanoscale 10 (2018) 13930–13935.
[74] Y. Sheng, J. Yang, F. Wang, L. Liu, H. Liu, C. Yan, Z. Guo, Sol-gel synthesized hexagonal boron nitride/titania nanocomposites with enhanced photocatalytic activity, Appl. Surface Sci. 465 (2019) 154–163.
[75] D. Pan, S. Ge, J. Zhao, et al., Synthesis and characterization of ZnNiIn layered double hydroxides derived mixed metal oxides with highly efficient photoelectrocatalytic activities, Indus. Eng. Chem. Res. 58 (2019) 836–848.
[76] R. Ge, X. Ren, X. Ji, Z. Liu, G. Du, A. Asiri, X. Sun, L. Chen, Benzoate anions-intercalated layered cobalt hydroxide nanoarray: an efficient electrocatalyst for oxygen evolution reaction, ChemSusChem 10 (2017) 4004–4008.
[77] H. Qi, M. Teng, M. Liu, et al., Biomass-derived nitrogen-doped carbon quantum dots: highly selective fluorescent probe for detecting Fe^{3+} ions and tetracyclines, J. Colloid Interf. Sci. 539 (2019) 332–341.
[78] C. Hou, Z. Tai, L. Zhao, Y. Zhai, Y. Hou, Y. Fan, F. Dang, J. Wang, H. Liu, High performance MnO@C microcages with a hierarchical structure and tunable carbon shell for efficient and durable lithium storage, J. Mater. Chem. A 6 (2018) 9723–9736.
[79] L. Chen, J. Zhao, L. Wang, et al., In-situ pyrolyzed polymethylsilsesquioxane multi-walled carbon nanotubes derived ceramic nanocomposites for electromagnetic wave absorption, Ceram. Int. (2019)https://doi.org/10.1016/j.ceramint.2019.03.052 in press.
[80] R. Li, X. Zhu, Q. Fu, G. Liang, Y. Chen, L. Luo, M. Dong, Q. Shao, C. Lin, R. Wei, Z. Guo, Nanosheet-based $Nb_{12}O_{29}$ hierarchical microspheres for enhanced lithium storage, Chem. Commun. 55 (2019) 2493–2496.
[81] W. Du, X. Wang, J. Zhan, et al., Biological cell template synthesis of nitrogen-doped porous hollow carbon spheres/MnO_2 composites for high-performance asymmetric supercapacitors, Electrochim. Acta 296 (2019) 907–915.
[82] L. Ma, Y. Zhu, M. Wang, X. Yang, G. Song, Y. Huang, Enhancing interfacial strength of epoxy resin composites via evolving hyperbranched amino-terminated POSS on carbon fiber surface, Compos. Sci. Technol. 170 (2019) 148–156.
[83] H. Zhu, W. Hu, Y. Xu, B. Wang, D. Zheng, Y. Fu, C. Zhang, G. Zhao, Z. Wang, Gradient structure based dual-robust superhydrophobic surfaces with high-adhesive force, Appl. Surface Sci. 463 (2019) 427–434.
[84] R. Wei, L. Tu, Y. You, C. Zhan, Y. Wang, X. Liu, Fabrication of crosslinked single-component polyarylene ether nitrile composite with enhanced dielectric properties, Polymer 161 (2019) 162–169.
[85] Y. He, Q. Chen, S. Yang, C. Lu, M. Feng, Y. Jiang, G. Cao, J. Zhang, C. Liu, Micro-crack behavior of carbon fiber reinforced Fe_3O_4/graphene oxide modified epoxy composites for cryogenic application, Compos. Part A 108 (2018) 12–22.